Advanced Journal of Chemistry, Section A

Journal homepage: www.ajchem-a.com

Original Research Article

Phytochemical Profiling and Computational Assessment of *Cissus verticillata* Bioactives Using GC–MS Against *Mycobacterium tuberculosis*

Sanjay Kumar Nayak[1], Neelam Sharma[2], Ganesh Meena B.[3]*, Yaso Deepika Mamidisetti[4], Rashmi Ranjan Sarangi[5], Rajendra Kumar Jadi[6], Murugesan Sudha[7], Divya Amaravadi[8], Jainendra Kumar Battineni[9]

[1] *College of Pharmaceutical Sciences, Marine Drive Road, Puri Odisha 752004, India*
[2] *Department, Pharmacology, Himachal Institute of Pharmaceutical Education and Research, Bela, Nadaun, Himachal Pradesh, India*
[3] *Arulmigu Kalasalingam College of Pharmacy, Krishnankoil, Virudhunagar 626002, Tamil Nadu, India*
[4] *Department of Pharmacology, School of Allied and Healthcare Sciences, Malla Reddy University, Maisammaguda, Hyderabad, Telangana - 500 100, India*
[5] *Royal College of Pharmacy and Health Sciences, Berhampur, Odisha 760002, India*
[6] *Department of Pharmaceutics, School of Pharmacy, Anurag University, Venkatapur, Ghatkesar, Medchal-Malkajgiri, Hyderabad - 500 088, Telangana, India*
[7] *Department of Pharmacology, Saveetha College of Pharmaceutical Sciences, Saveetha Institute of Medical and Technical Sciences (SIMATS), Deemed University, Chennai, Tamil Nadu, India*
[8] *Department of Pharmacy Practice, Saveetha College of Pharmaceutical Sciences, Saveetha Institute of Medical and Technical Sciences (SIMATS), Deemed University, Chennai, Tamil Nadu, India*
[9] *Department of Pharmaceutical Chemistry, School of Pharmacy, Anurag University, Venkatapur, Ghatkesar, Medchal-Malkajgiri, Hyderabad-500 088, Telangana, India*

ARTICLEINFO

Article history

Submitted: 2025-11-24
Revised: 2025-12-27
Accepted: 2026-01-07
ID: AJCA-2511-1978
DOI: 10.48309/AJCA.2026.561857.1978

KEYWORDS

Cissus verticillata
Phytochemical profiling
Anti-tubercular activity
Molecular docking
MurG glycosyltransferase
ADMET prediction

ABSTRACT

This study investigated the phytochemical composition and antitubercular potential of *Cissus verticillata* using an integrated gas chromatography mass spectroscopy (GC–MS), molecular docking, and ADMET approach. The authenticated hydroalcoholic extract showed a dark brown to greenish-brown appearance, a yield of 10.95%, near-neutral pH, and the absence of foreign matter, heavy metals, pesticide residues, and pathogenic microorganisms, confirming its suitability for pharmacological use. Preliminary phytochemical screening indicated a rich metabolite profile with strong presence of alkaloids, flavonoids, and phenolic compounds, along with moderate levels of saponins and tannins. GC–MS analysis identified 55 phytochemical constituents, with major compounds, including L-prolyl-L-valine (13.28%), 3,6-diisopropylpiperazin-2,5-dione (4.72%), hydrocinnamic acid (3.84%), and tyrosol (2.39%), supported by minor sterols, esters, and phenolics, which contribute to chemical diversity. Molecular docking against Mycobacterium tuberculosis MurG glycosyltransferase (PDB ID: 2WGE) revealed strong binding affinities for squalene (–8.3 kcal/mol), loliolide (–7.2 kcal/mol), quinic acid (–7.1 kcal/mol), and methyl-*N*-hydroxybenzenecarboximidate (–7.0 kcal/mol), surpassing or matching the native ligand. Key hydrophobic and hydrogen bond interactions were observed with PHE404, HIS311, PRO280, and GLY403. The ADMET analysis highlighted loliolide, maltol, 5-hydroxymethylfurfural, and quinic acid as drug-like candidates with favorable solubility, absorption, low toxicity, and minimal environmental bioaccumulation. Collectively, these findings position *Cissus verticillata* as a promising source of antitubercular lead compounds, warranting further experimental validation.

* Corresponding author: Meena B., Ganesh
✉ E-mail: bgmeena2000@gmail.com

GRAPHICAL ABSTRACT

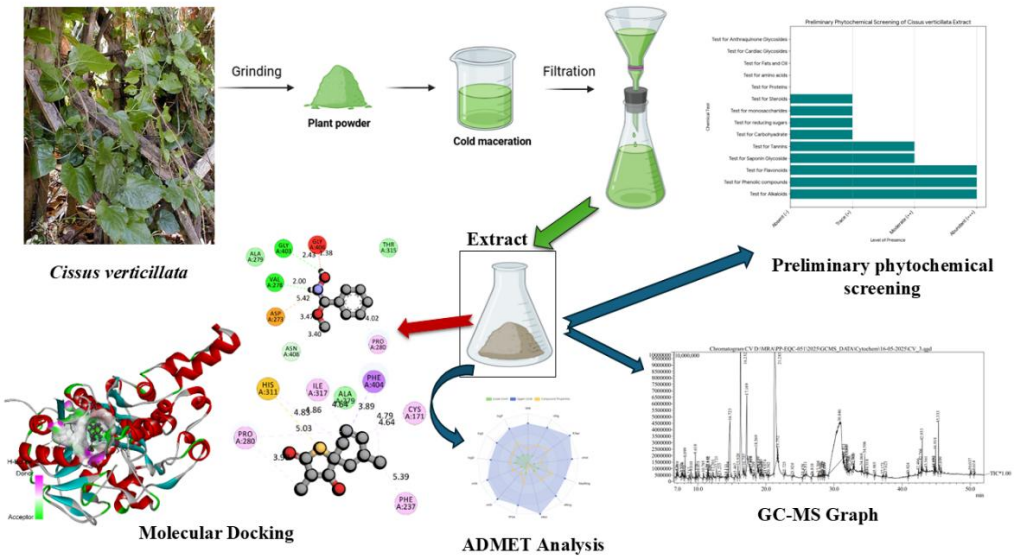

Introduction

Tuberculosis (TB) is a major global health challenge caused by the persistent and highly adaptable pathogen Mycobacterium tuberculosis [1,2]. Despite the availability of established first-line and second-line treatment regimens, the increasing incidence of multidrug-resistant (MDR) and extensively drug-resistant (XDR) TB has intensified the demand for novel therapeutic agents [3–5]. Natural products have long served as indispensable reservoirs of structurally diverse and biologically active molecules, making medicinal plants particularly valuable in the search for alternative antimycobacterial compounds. Among these, *Cissus verticillata* has emerged as a traditionally significant species with a wide spectrum of reported medicinal uses [6,7].

Cissus verticillata, a climber belonging to the Vitaceae family, has been employed in various traditional healing systems due to its anti-inflammatory, antimicrobial, antidiabetic, and wound healing properties. These therapeutic applications are attributed to its rich phytochemical composition, which includes phenolics, flavonoids, glycosides, terpenoids, fatty acid derivatives, and other secondary metabolites that are known for their biological efficacy. The scientific exploration of such plants requires systematic analytical approaches to identify and characterize the chemical constituents responsible for their pharmacological properties [8–11].

Gas chromatography-mass spectrometry (GC–MS) is a robust analytical technique widely used for phytochemical investigation due to its precision, sensitivity, and ability to detect volatile and semi-volatile compounds within complex plant matrices. By providing detailed chemical profiles, GC–MS aids in establishing the phytochemical identity of plant extracts and supports the discovery of bioactive molecules that may contribute to antimicrobial activity. This analytical foundation is essential for advancing further biological and computational assessments [12,13].

Computational analysis has become an integral part of modern drug discovery, offering a rapid, cost-effective, and reliable means of predicting the biological potential of identified phytocompounds. Techniques such as molecular docking, interaction profiling, and absorption, distribution, metabolism, excretion, and toxicity (ADMET) predictions help assess the

pharmacological relevance of plant-derived molecules [14,15]. These *in silico* approaches allow for the simultaneous screening of multiple compounds, identifying those with favorable binding characteristics, optimal pharmacokinetics, and safety profiles. Such predictive tools significantly reduce the experimental workload and streamline the prioritization of promising candidates for future wet lab evaluations [16].

Integrating phytochemical profiling with computational methods provides a comprehensive framework for exploring medicinal plants such as *Cissus verticillata*. This combined approach bridges traditional knowledge with contemporary scientific techniques, thereby supporting the identification of plant-derived compounds with potential therapeutic importance. The present study focused on the GC–MS-based phytochemical profiling of *Cissus verticillata* and the computational evaluation of its identified bioactive compounds, aiming to explore their possible application against Mycobacterium tuberculosis and contribute to the development of new, effective anti-TB strategies.

Materials and Methods

Collection and extraction of cissus verticillata herb

Cissus verticillata was collected in December 2024 from the local regions of Buldhana, Maharashtra, India. For extraction, the plant material was thoroughly washed, shade-dried at room temperature, and coarsely powdered using a mechanical grinder. The dried powder was subjected to maceration, a cold extraction technique widely used to preserve thermolabile phytoconstituents. The powdered sample was soaked in an appropriate solvent at a fixed drug-to-solvent ratio (1:5–1:10 w/v) and kept undisturbed at room temperature for 72 h with occasional shaking to enhance the solvent penetration and diffusion. After maceration, the mixture was filtered through muslin cloth, followed by Whatman No. 1 filter paper. The filtrate was then concentrated under reduced pressure using a rotary evaporator and finally dried to obtain a crude extract, which was stored in an airtight container at 4 °C until further analysis [17–19]. Following extraction, the obtained crude hydroalcoholic extract was subjected to physicochemical and preliminary phytochemical evaluations to assess its quality, purity, and the presence of major classes of bioactive constituents prior to advanced analytical characterization.

Physicochemical and phytochemical evaluation

The physicochemical parameters of dried and powdered *Cissus verticillata* were evaluated following standard pharmacopoeial guidelines. Moisture content was determined by drying the sample at 105°C to constant weight. The total ash, acid-insoluble ash, and water-soluble ash values were measured by controlled incineration of the powdered drug. The alcohol-soluble and water-soluble extractive values were assessed by macerating the plant powder in the respective solvents, followed by filtration and evaporation to dryness. These parameters were used to assess the purity, quality, and stability of crude plant material [20,21].

The crude extract obtained from maceration was subjected to a preliminary phytochemical screening to identify the major classes of bioactive constituents. Standard qualitative tests were performed for alkaloids, flavonoids, tannins, phenolics, glycosides, saponins, terpenoids, steroids, carbohydrates, proteins, and amino acids using appropriate reagents, such as Mayer's, Dragendorff's, ferric chloride, Salkowski, and Molisch tests. Observations such as color changes or precipitate formation were recorded to confirm the presence of these phytochemical groups [22,23]. While preliminary phytochemical screening provided qualitative evidence of major

metabolite classes, detailed identification and structural characterization of individual bioactive compounds requires further analysis using GC–MS.

Microbial determination

The microbial quality of the extracts was assessed using the pour-plate method. One gram of powdered sample or an equivalent volume of liquid extract was diluted in sterile distilled water, followed by serial dilution. Aliquots were plated on nutrient agar, cetrimide nutrient agar, salt nutrient agar, MacConkey agar, and incubated at 37 °C for 24 h. Fungal contamination was evaluated using Sabouraud dextrose agar incubated at 27 °C for 72 h. Colony-forming units (CFU) were counted, and values were recorded as the mean of duplicate readings. Specific microbial contaminants were screened using the enrichment and selective media. Escherichia coli was detected by enrichment in nutrient broth, followed by inoculation into MacConkey broth. Salmonella spp. was enriched in nutrient broth, transferred to selenite and tetrathionate broth, and streaked on deoxycholate citrate agar. Shigella spp. were enriched in nutrient broth (pH 8.0) and plated on Salmonella–Shigella agar, with further confirmation using TSI tests. Pseudomonas aeruginosa was isolated through soybean–casein digest medium and cetrimide agar, whereas Staphylococcus aureus was identified by growth on Mannitol Salt Agar followed by catalase and coagulase testing [24,25].

GC–MS analysis

The methanolic extract of *Cissus verticillata* was analyzed using a GC–MS system operated under the laboratory's standard phytochemical scan method (PHYTOCHEM_Scan_1). A 1.0 µL aliquot of the sample (Vial 1) was injected according to the programmed injection conditions saved within the method file. Data acquisition was performed in full-scan electron ionization (EI) mode using the instrument's tuned parameters documented in the accompanying method report. Chromatographic separation and mass spectral acquisition were performed following the temperature program, ion source settings, and mass scan range predefined in the PHYTOCHEM_Scan_1 method. The total ion chromatogram and mass spectra were automatically processed using instrument software, with peak detection, integration, and spectral matching performed using the built-in NIST library search. All analyses were conducted using the same operating method and tuning file to ensure consistency in the identification of the phytoconstituents [26–28].

Computational analysis

Molecular docking

Computational docking was performed to evaluate the interaction of GC–MS–identified phytoconstituents of *Cissus verticillata* with the Mycobacterium tuberculosis target protein (PDB ID: 2WGE) (Figure 1). The chemical structures of the selected compounds were drawn and optimized using ChemDraw, and their corresponding 2D/3D formats were retrieved from PubChem when available. The target protein structure was downloaded from the RCSB PDB and prepared by removing water molecules, adding polar hydrogen atoms, and optimizing amino acid residues using Discovery Studio. Ligand energy minimization and conversion to the required docking formats were performed using PyRx with atomic attributes based on XYZ coordinates (*e.g.,* 38.098000, 0.998857, –6.776000). Docking simulations were conducted in the PyRx AutoDock Vina environment using default grid parameters centered on the active site of the 2WGE. Binding affinities and interaction profiles were generated, and protein–ligand complexes were visualized and analyzed using Discovery Studio Visualizer [29–32].

Figure 1. 3D ribbon view of Mycobacterium tuberculosis targeted protein (PDB ID: 2WGE) with native ligand

ADMET analysis

The pharmacokinetic and toxicity parameters of the docked phytoconstituents were evaluated using standard *in silico* ADMET prediction tools. Structures were sketched and refined using ChemDraw with canonical SMILES obtained from PubChem. Drug-likeness, physicochemical properties, gastrointestinal absorption, lipophilicity, and other pharmacokinetic descriptors were predicted using SwissADME. Toxicological and advanced ADMET profiles, including hepatotoxicity, hERG inhibition, cytochrome interactions, and safety parameters, were evaluated using the ADMETlab 3.0. All predictions were recorded to assess the suitability of the identified compounds as potential antitubercular candidates [33,34].

Results and Discussion

Organoleptic, physicochemical, and microbial evaluation

The hydroalcoholic extract of *Cissus verticillata* displayed characteristic plant-derived features, with a dark brown to greenish-brown color, an earthy herbal odor, and a bitter, slightly astringent taste. The extract was solid in texture and produced a yield of 10.95%. Physicochemical assessment showed near-neutral pH values (7.2 for 1% and 6.9 for 10% solutions) and an acceptable moisture content (LOD: 6.5%). The extract contained 3.44% total ash, with minimal acid-insoluble matter (0.12%) and moderate water-soluble and sulfated ash values (4.24% and 2.32%, respectively). The extractive values indicated higher solubility in water (13.25%) than in alcohol (8.97%). No foreign matter, heavy metals, or pesticide residues were detected, which confirmed the purity and suitability of the extract for further analysis. Microbial evaluations revealed the absence of major pathogenic contaminants. Tests for Escherichia coli, Salmonella spp., Shigella spp., Pseudomonas aeruginosa, and Staphylococcus aureus were negative, confirming that the extract met microbiological safety standards and was free from harmful microorganisms.

Preliminary phytochemical screening

Preliminary phytochemical analysis of the *Cissus verticillata* hydroalcoholic extract of *C. verticillata* revealed a diverse profile of secondary metabolites (Figure 2).

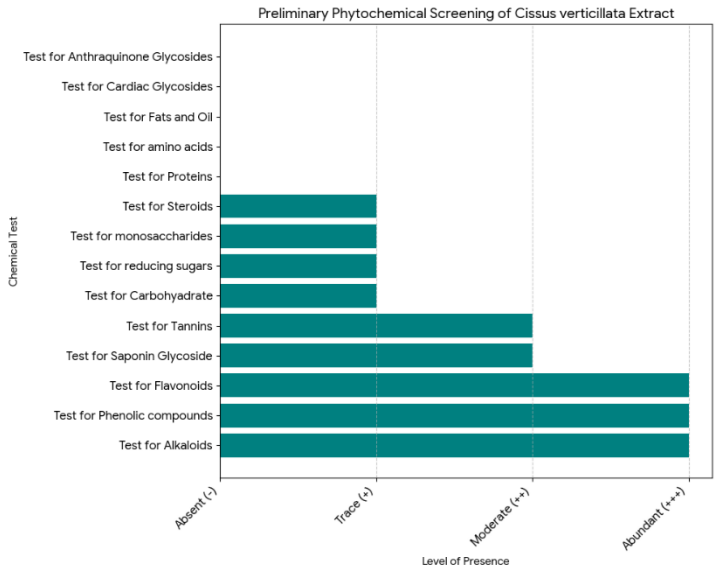

Figure 2. The results of preliminary phytochemical screening of *Cissus verticillata* extract

Alkaloids, flavonoids, and phenolic compounds were strongly present (+++), indicating rich antioxidant and bioactive composition. Moderate levels of saponins and tannins (++) further suggest potential antimicrobial, astringent, and immunomodulatory activity. Trace amounts of steroids and carbohydrate-related constituents, including reducing sugars and monosaccharides, were also detected (+), supporting the presence of primary metabolites that may contribute to the overall extract stability and bioactivity.

In contrast, proteins, amino acids, fats and oils, anthraquinone glycosides, and cardiac glycosides were absent, highlighting the dominance of non-nitrogenous and polyphenolic constituents as major chemical contributors. This phytochemical profile emphasizes the therapeutic relevance of the extract, particularly because of the abundant phenolics, alkaloids, and flavonoids, which are commonly associated with antitubercular, anti-inflammatory, and free radical scavenging properties. Based on the metabolite-rich phytochemical profile observed, GC–MS analysis was performed to elucidate the individual chemical constituents responsible for the biological potential of the extract.

GC–MS analysis

GC–MS analysis of the hydroalcoholic extract of Cissus verticillata was performed using a gas chromatography–mass spectrometry system operated under the validated laboratory method PHYTOCHEM_Scan_1. Separation was achieved on a capillary column (HP-5MS type, 5% phenyl–95% dimethylpolysiloxane) with dimensions of 30 m × 0.25 mm internal diameter and 0.25 µm film thickness. High-purity helium was used as the carrier gas at a constant flow rate of 1.0 mL/min. A 1.0 µL aliquot of the extract was injected in split mode, and the injector temperature was maintained at 250 °C. The oven temperature program was initiated at 60 °C, held for 2 min, followed by a gradual increase at 10 °C/min to 280 °C, where it was held for 10 min, allowing efficient elution of both low- and high-boiling phytoconstituents. The total run time was 52 min. Mass spectrometric detection was carried out using an electron ionization (EI) source operated at 70 eV, with the ion source temperature set at 230 °C and the quadrupole temperature maintained at 150 °C. Data were acquired in full-scan mode over a mass range of m/z 40–500, ensuring the comprehensive detection of volatile

and semi-volatile compounds. The instrument was tuned using the standard tuning file AT_AFTER PM_NORMAL_F1_CID, and data acquisition and processing were performed using the proprietary GC–MS software integrated with the NIST 20 mass spectral library for compound identification. Peaks were identified based on a combination of retention time, mass spectral fragmentation patterns, and library similarity indices, with only well-matched compounds considered for interpretation The most abundant bioactive molecule identified was quinic acid, followed by catechol, 5-hydroxymethylfurfural, 4*H*-pyran-4-one derivative (maltol), and hydroquinone, which collectively contribute to the strong antioxidant and biological potential of the extract. Additional minor compounds include furaneol, squalene, loliolide, methyl *N*-hydroxybenzenecarboximidate, and 3,4,5-trimethylphenol, each of which has documented biological relevance. The overall chemical composition confirmed the presence of phytoconstituents responsible for the antioxidant, anti-inflammatory, antimicrobial, and cytoprotective properties, reinforcing the therapeutic value of the plant extract (Table 1).

The chromatographic pattern demonstrated that quinic acid (33.36%) was the dominant phytochemical, reflecting its crucial role in plant biosynthesis and antioxidant defense (Figure 3). Catechol (14.28%) further strengthened the phenolic content of the extract, indicating a high free-radical scavenging capacity. Maillard-derived molecules such as 5-hydroxymethylfurfural and 4*H*-pyran-4-one derivatives add to the antioxidant and antimicrobial potential, while Hydroquinone contributes additional redox-active activity.

Table 1. GC–MS Identified Compounds from the Extract

Compound name	Retention time (min)	Area (%)	Rationale
Quinic acid	30.85	33.36	Major bioactive, antioxidant, precursor in shikimic acid pathway
Catechol	16.25	14.28	Strong antioxidant, polyphenolic compound found in plants
5-Hydroxymethylfurfural	17.19	5.30	Maillard reaction product with antioxidant properties
4*H*-Pyran-4-one derivative (Maltol)	14.72	6.47	Has potential antioxidant and flavor-enhancing properties
Hydroquinone	18.57	2.68	Used in cosmetics and pharmaceuticals, potent antioxidant
Furaneol	12.20	0.31	Sweet flavoring compound with biological activity
Squalene	45.70	0.11	Precursor in steroid biosynthesis, skin protective agent
Loliolide	32.02	0.09	Lactone compound with antioxidant and cytotoxic activity
Methyl *N*-hydroxybenzenecarboximidate	7.57	0.16	Potential synthetic intermediate with biological significance
Phenol, 3,4,5-trimethyl-	19.45	0.06	Phenolic compound possibly with antimicrobial traits

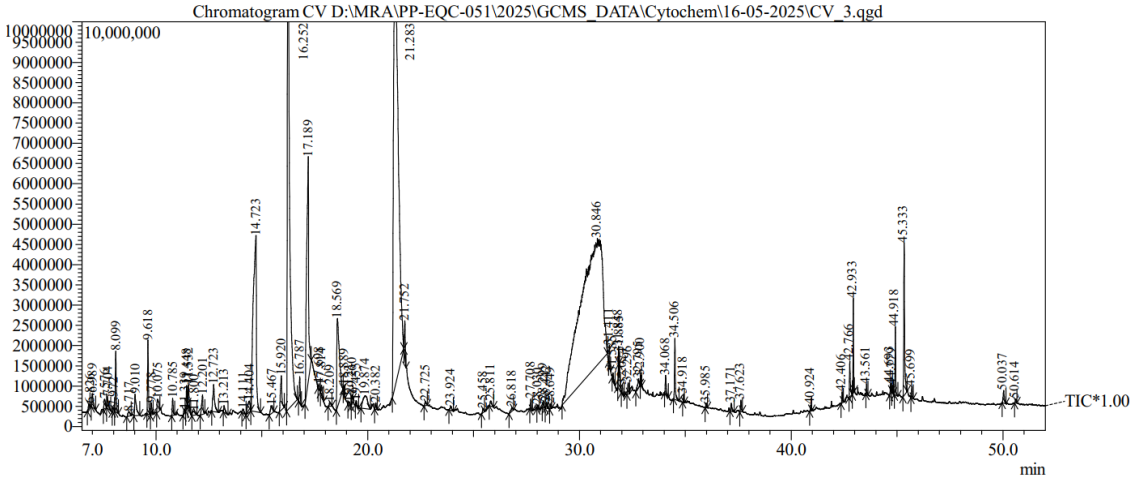

Figure 3. GC-MS graph of *Cissus verticillata* extract

Minor compounds, such as Loliolide, Squalene, and Furaneol, indicate the presence of lactones, terpenoids, and natural aroma compounds that enhance bioactivity and skin-protective functions. Trace levels of oxime derivatives and trimethylphenols reflect the additional biochemical diversity. The presence of sterol- and lipid-related metabolites supports membrane stabilizing and anti-inflammatory properties.

Collectively, the GC–MS profile confirmed that the extract was rich in phenolics, organic acids, Maillard reaction derivatives, lactones, and minor terpenoids, all of which synergistically contributed to its antioxidant, antimicrobial, anti-inflammatory, and cytoprotective properties. These findings validate the pharmacological relevance of this plant and support its traditional and therapeutic applications.

Computational analysis

Molecular docking

Molecular docking analysis of GC-MS-identified bioactive compounds from *Cissus verticillata* against Mycobacterium tuberculosis (PDB ID: 2WGE) revealed diverse interaction patterns, with several compounds demonstrating comparable—or in some cases superior—binding affinity relative to the native ligand NL-2WGE. Binding interactions of selected compounds with Mycobacterium tuberculosis are tabulated in Table 2. 2D and 3D interaction diagrams are illustrated in Table 3. The native ligand showed a docking score of −7.0 kcal/mol, driven predominantly by hydrophobic interactions, especially π-sigma and π-alkyl contacts involving residues PHE404, PRO280, HIS311, ILE317, and PHE237. Therefore, these residues represent key pharmacophoric hotspots in the active site. 5-Hydroxymethylfurfural showed a moderate docking score (−5.4 kcal/mol) and differed mechanistically from the native ligand by forming multiple hydrogen bonds with GLY403, HIS407, and PHE404. Although energetically weaker than that of NL-2WGE, the presence of strong hydrogen bond donors and acceptors suggests a distinct but stable binding orientation. Catechol exhibited a similar binding score (−5.3 kcal/mol) and maintained both hydrogen bonding (HIS345) and π−π stacking (PHE404). However, its interaction network was less extensive than that of the native ligand, resulting in relatively lower stability. Furaneol also demonstrated a comparable binding score (−5.3 kcal/mol) but displayed a rich network of hydrophobic interactions with HIS311, PRO280, and PHE402, supplemented by two hydrogen bonds. Its binding cavity engagement is broader than that of catechol but

still inferior to that of NL-2WGE. Hydroquinone showed a slightly lower affinity (–5.1 kcal/mol), driven by a dominant hydrogen bond with GLY403 and limited hydrophobic contacts. Its minimal interaction counts likely contributed to its lower stability relative to that of the native ligand. Loliolide presented a noticeably high docking score (–7.2 kcal/mol), surpassing that of the native ligand. Notably, it preserved the key π-sigma interaction with PHE404, a signature interaction of NL-2WGE, and strong hydrophobic interactions with PRO280 and HIS311. The preservation of native binding motifs explains the superior docking affinity. Maltol (–5.3 kcal/mol) demonstrated moderate hydrogen bonding along with hydrophobic stabilization; however, its interaction profile remained weaker than that of the native ligand. Methyl-*N*-hydroxybenzenecarboximidate achieved a high score (–7.0 kcal/mol), identical to NL-2WGE. Its binding is dominated by hydrogen bonds (VAL278 and GLY403) and electrostatic attraction with ASP273, in addition to π-alkyl hydrophobic contacts. The presence of both polar and nonpolar interactions indicated a balanced and stable binding pattern that mimicked, but did not surpass, the native ligand. Phenol, 3,4,5-trimethyl- showed improved affinity (–6.1 kcal/mol) and multiple hydrophobic interactions involving PHE404, HIS311, and PRO280. Although devoid of extensive hydrogen bonding, strong aromatic and alkyl interactions enhanced the fit within the binding pocket. Quinic acid produced a very high docking score (–7.1 kcal/mol), facilitated by multiple strong hydrogen bonds with HIS407, GLY318, GLY406, and a π-donor hydrogen bond with PHE404. This molecule exhibits the most extensive hydrogen bond network, which likely stabilizes its binding conformation and enhances its affinity. Squalene displayed the strongest binding affinity (–8.3 kcal/mol), significantly surpassing the native ligand. The interaction profile was dominated entirely by hydrophobic interactions involving a large number of residues (CYS171, PRO280, ALA287, ALA321, MET213, ILE317, HIS311, HIS345, PHE402, and PHE404). The bulky triterpenoid nature of squalene provides an extended hydrophobic surface area, making it exceptionally compatible with the hydrophobic pocket of 2WGE. Despite the lack of hydrogen bonding, the sheer magnitude of the hydrophobic contacts resulted in the most stable docking geometry among the tested compounds.

Collectively, these findings suggest that loliolide, quinic acid, methyl-*N*-hydroxybenzenecarboximidate, and particularly squalene, display binding energies comparable to or better than those of NL-2WGE. Compounds with high hydrophobic surface areas (*e.g.,* squalene and loliolide) or strong hydrogen bond capacity (*e.g.,* quinic acid) demonstrated superior affinity, indicating distinct but effective binding strategies for targeting the 2WGE active site. Therefore, these candidates may serve as promising lead molecules for further antitubercular optimization and *in vitro* validation.

Table 2. Binding interactions of selected compounds with Mycobacterium tuberculosis

Amino acid	Bond length	Bond type	Bond category	Ligand energy (Kcal/mol)	Docking score
			NL-2WGE		
PHE404	3.89437	Hydrophobic	π-Sigma	102.09	-7
HIS311	4.8282	Other	π-Sulfur		
CYS171	4.63964	Hydrophobic	Alkyl		
PRO280	3.90094	Hydrophobic	Alkyl		

Amino acid	Bond length	Bond type	Bond category	Ligand energy (Kcal/mol)	Docking score
PRO280	5.03127	Hydrophobic	Alkyl		
ILE317	4.64117	Hydrophobic	Alkyl		
PHE237	5.38589	Hydrophobic	Π-Alkyl		
HIS311	4.86018	Hydrophobic	π-Alkyl		
PHE404	4.78919	Hydrophobic	π-Alkyl		
5-Hydroxymethylfurfural					
GLY403	2.0373	Hydrogen Bond	Conventional Hydrogen Bond	198.58	-5.4
HIS407	2.76555	Hydrogen Bond	Conventional Hydrogen Bond		
PHE404	2.44003	Hydrogen Bond	Conventional Hydrogen Bond		
HIS311	3.60922	Hydrogen Bond	Carbon Hydrogen Bond		
PRO280	4.22976	Hydrophobic	π-Alkyl		
Catechol					
HIS345	2.52743	Hydrogen Bond	Conventional Hydrogen Bond	48.11	-5.3
PHE404	4.02717	Hydrophobic	π-π Stacked		
CYS171	5.436	Hydrophobic	π-Alkyl		
PRO280	5.17541	Hydrophobic	π-Alkyl		
Furaneol					
CYS171	2.82037	Hydrogen Bond	Conventional Hydrogen Bond	240.05	-5.3
PHE402	3.09311	Hydrogen Bond	Conventional Hydrogen Bond		
HIS311	4.57859	Hydrophobic	π-π T-shaped		
PRO280	3.91061	Hydrophobic	Alkyl		
PRO280	4.91322	Hydrophobic	π-Alkyl		
HIS311	5.32096	Hydrophobic	π-Alkyl		
HIS311	5.13923	Hydrophobic	π-Alkyl		
HIS345	5.2412	Hydrophobic	π-Alkyl		
PHE402	5.10016	Hydrophobic	π-Alkyl		
PHE404	4.35734	Hydrophobic	π-Alkyl		
Hydroquinone					
GLY403	2.94401	Hydrogen Bond	Conventional Hydrogen Bond	45.69	-5.1
HIS311	5.05811	Hydrophobic	π-πT-shaped		
PRO280	4.4591	Hydrophobic	π-Alkyl		
Loliolide					
PHE404	3.89311	Hydrophobic	π-Sigma	184.92	-7.2
PRO280	3.87253	Hydrophobic	Alkyl		
CYS171	4.53639	Hydrophobic	Alkyl		
HIS311	5.01292	Hydrophobic	π-Alkyl		
PHE404	4.5586	Hydrophobic	π-Alkyl		
PHE404	4.89	Hydrophobic	π-Alkyl		
Maltol					
GLY318	3.46982	Hydrogen Bond	Carbon Hydrogen Bond	54.85	-5.3
HIS311	4.78507	Hydrophobic	π-π T-shaped		
PRO280	3.97755	Hydrophobic	Alkyl		
PRO280	4.71195	Hydrophobic	π-Alkyl		

Amino acid	Bond length	Bond type	Bond category	Ligand energy (Kcal/mol)	Docking score
HIS311	5.3601	Hydrophobic	π-Alkyl		
PHE402	5.27006	Hydrophobic	π-Alkyl		
Methyl_*N*-hydroxybenzenecarboximidate					
ASP273	5.41647	Electrostatic	Attractive Charge	92.51	-7
VAL278	2.0033	Hydrogen Bond	Conventional Hydrogen Bond		
GLY403	2.42522	Hydrogen Bond	Conventional Hydrogen Bond		
ASP273	3.46885	Hydrogen Bond	Carbon Hydrogen Bond		
ASN408	3.39643	Hydrogen Bond	Carbon Hydrogen Bond		
PRO280	4.02242	Hydrophobic	π-Alkyl		
Phenol, 3,4,5-trimethyl-					
VAL278	2.88093	Hydrogen Bond	Conventional Hydrogen Bond	58.17	-6.1
PHE404	5.40471	Hydrophobic	π-πT-shaped		
PRO280	4.0482	Hydrophobic	Alkyl		
PRO280	3.99224	Hydrophobic	π-Alkyl		
HIS311	4.62739	Hydrophobic	π-Alkyl		
HIS311	5.41049	Hydrophobic	π-Alkyl		
PHE402	4.68754	Hydrophobic	π-Alkyl		
PHE404	4.43333	Hydrophobic	π-Alkyl		
Quinic_acid					
HIS407	2.63251	Hydrogen Bond	Conventional Hydrogen Bond	1439.43	-7.1
GLY318	2.2767	Hydrogen Bond	Conventional Hydrogen Bond		
GLY318	3.386	Hydrogen Bond	Carbon Hydrogen Bond		
GLY406	3.19497	Hydrogen Bond	Carbon Hydrogen Bond		
PHE404	3.29933	Hydrogen Bond	π-Donor Hydrogen Bond		
Squalene					
CYS171	4.76226	Hydrophobic	Alkyl	94.18	-8.3
PRO280	4.28151	Hydrophobic	Alkyl		
PRO280	4.42071	Hydrophobic	Alkyl		
ALA321	3.48773	Hydrophobic	Alkyl		
ALA287	3.27714	Hydrophobic	Alkyl		
ALA321	3.50136	Hydrophobic	Alkyl		
ALA325	4.16913	Hydrophobic	Alkyl		
ALA215	3.80383	Hydrophobic	Alkyl		
MET213	4.36136	Hydrophobic	Alkyl		
VAL278	5.35079	Hydrophobic	Alkyl		
ILE317	4.60258	Hydrophobic	Alkyl		
PRO316	3.7761	Hydrophobic	Alkyl		
ILE317	3.832	Hydrophobic	Alkyl		
HIS311	4.74859	Hydrophobic	π-Alkyl		
HIS345	4.8811	Hydrophobic	π-Alkyl		
PHE402	4.45031	Hydrophobic	π-Alkyl		
PHE402	5.00108	Hydrophobic	π-Alkyl		
PHE404	4.30386	Hydrophobic	π-Alkyl		

Table 3. 2D and 3D interaction diagrams illustrating the binding modes of the selected phytochemicals and native ligands within the MurG active site

3D Interactions	2D Interactions
NL-2WGE	
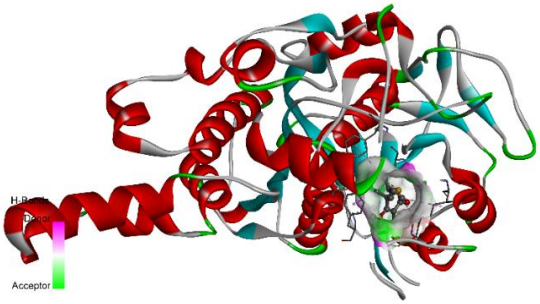	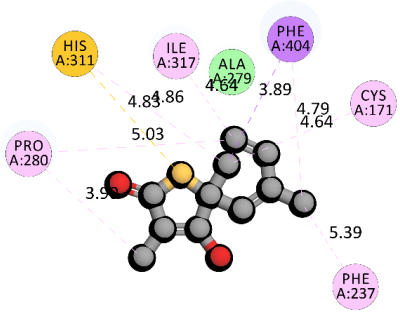
5-Hydroxymethylfurfural	
	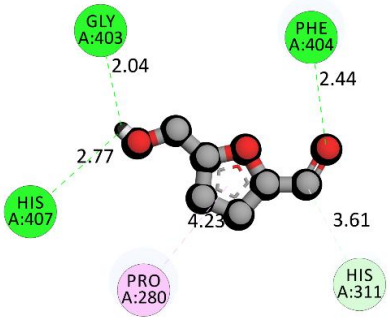
Catechol	
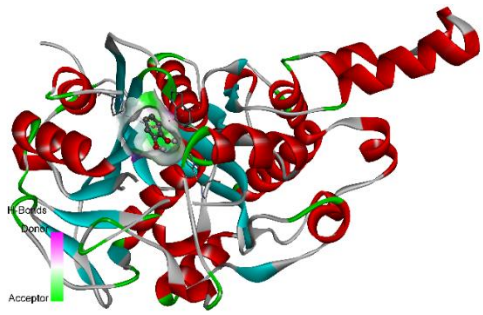	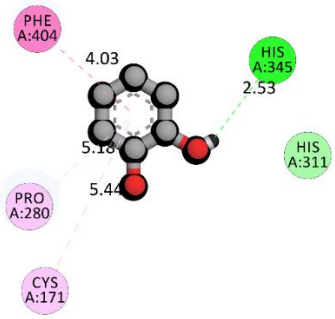
Furaneol	
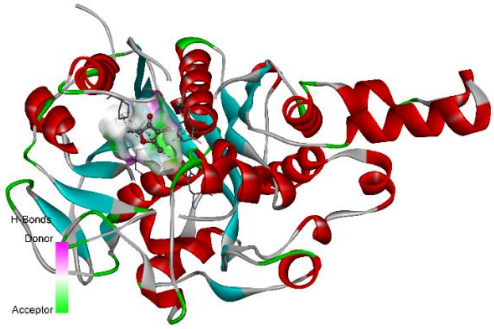	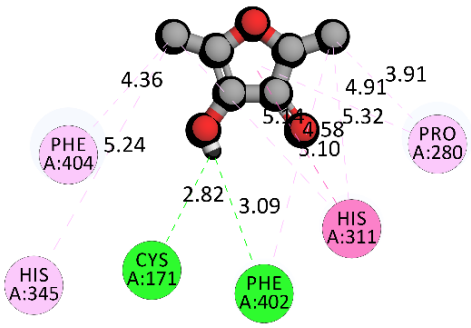

Hydroquinone

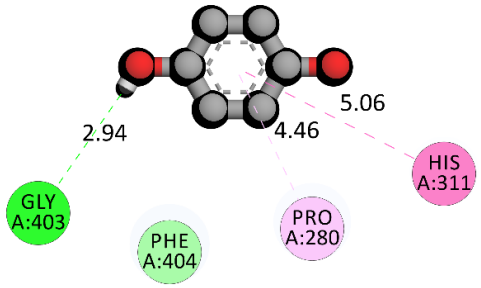

Loliolide

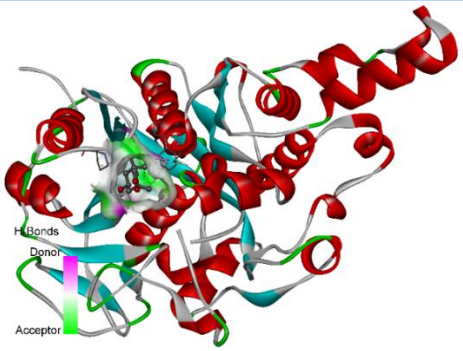

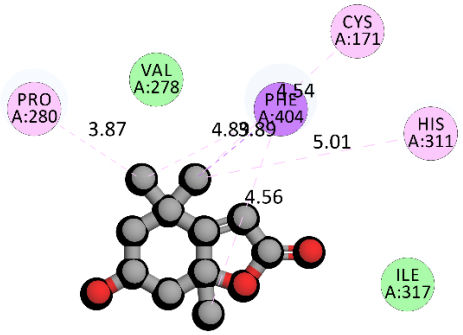

Maltol

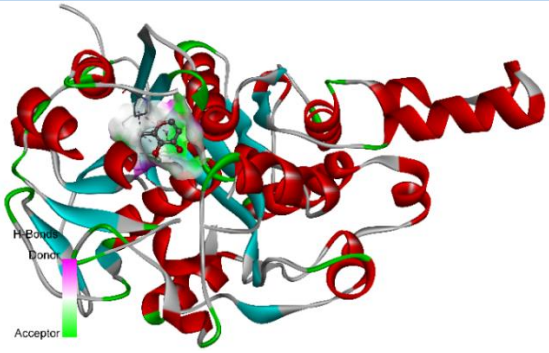

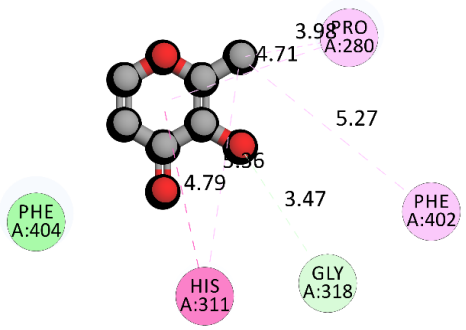

Methyl_*N*-hydroxybenzenecarboximidate

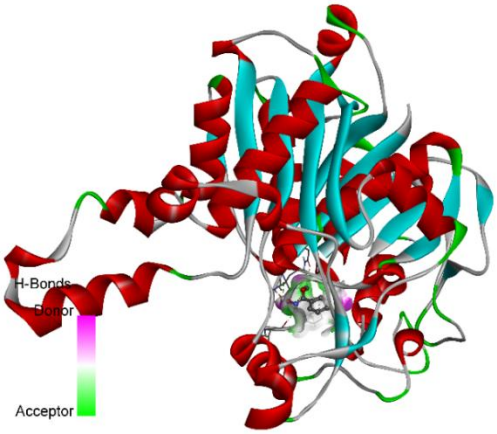

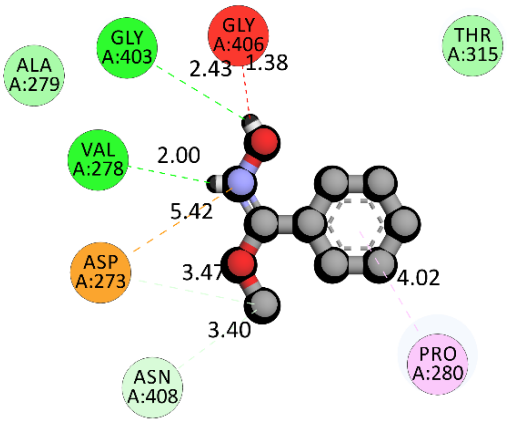

Phenol, 3,4,5-trimethyl-

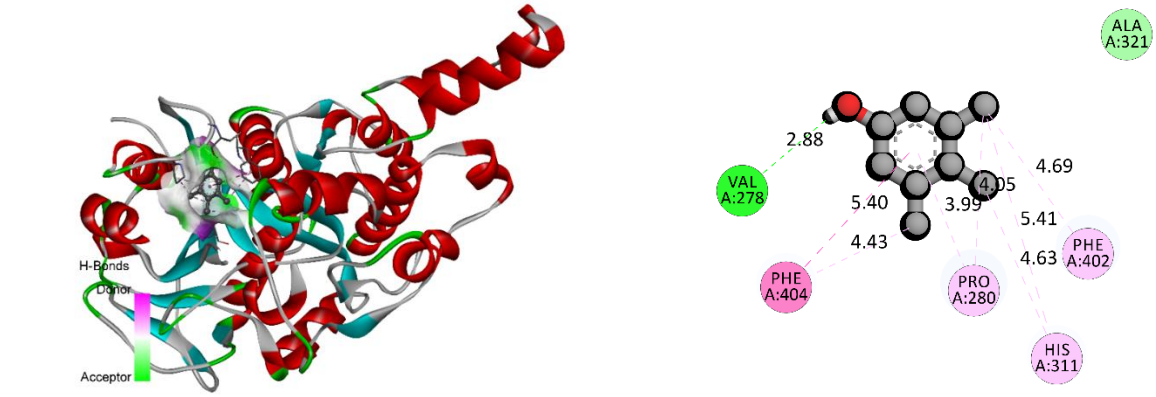

Quinic_acid

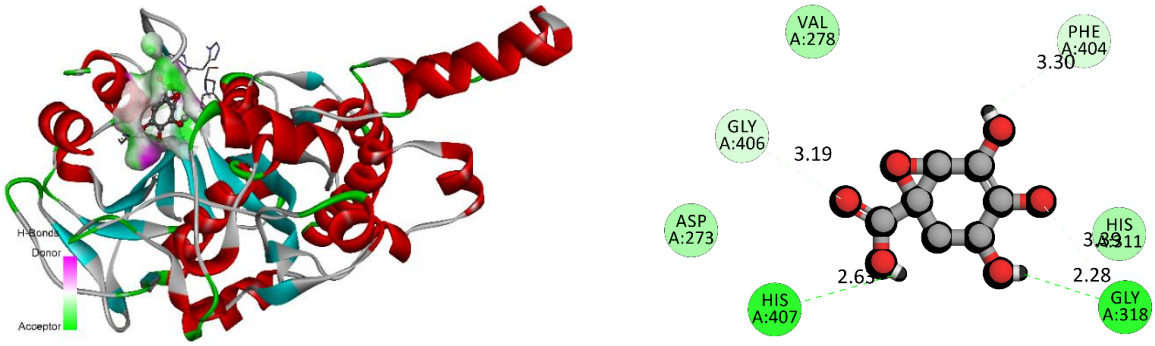

Squalene

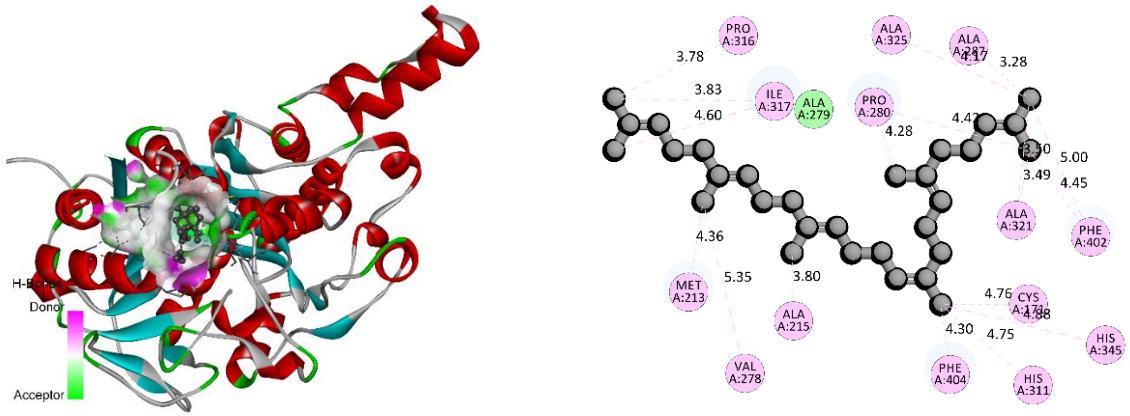

ADMET analysis

The ADMET profiling of the GC–MS–identified compounds from *Cissus verticillata* revealed diverse pharmacokinetic and toxicity characteristics when compared with the native ligand (NL-2WGE). Overall, physicochemical assessment demonstrated that most compounds fell within acceptable drug-like ranges and possessed improved solubility and structural flexibility relative to the native ligand. The physicochemical assessment showed that most *Cissus verticillata* compounds fell within acceptable drug ranges and displayed improved solubility and polarity compared with the native ligand NL-2WGE (Table 4).

Table 4. Physicochemical properties of selected derivatives

Compounds	MW	Volume	Dense	nHA	nHD	nRot	nRing	TPSA	logS	logP
NL-2WGE	210.07	215.7995	0.97345	2	1	2	1	37.3	-2.74729	2.476737
5-Hydroxymethylfurfural	126.03	122.2372	1.031028	3	1	2	1	50.44	0.16153	0.405887
Catechol	110.04	113.447	0.969968	2	2	0	1	40.46	0.526148	1.025353
Furaneol	128.05	124.8737	1.025436	3	1	0	1	46.53	-0.15822	0.063934
Hydroquinone	110.04	113.447	0.969968	2	2	0	1	40.46	-0.58178	0.589621
Loliolide	196.11	202.7971	0.967025	3	1	0	2	46.53	-2.89296	1.347597
Maltol	126.03	122.2372	1.031028	3	1	0	1	50.44	-0.8513	-0.15746
Methyl_*N*-hydroxybenzenecarboximidate	151.06	156.3993	0.965861	3	1	2	1	41.82	-1.87037	2.151765
Phenol, 3,4,5-trimethyl-	136.09	156.5447	0.869336	1	1	0	1	20.23	-2.14296	2.690494
Quinic_acid	192.06	171.1768	1.121998	6	5	1	1	118.22	-0.2177	-1.01873
Squalene	410.39	511.6173	0.802143	0	0	15	0	0	-10.5308	11.16941

NL-2WGE exhibited moderate lipophilicity (logP 2.47), low polarity (TPSA 37.3 Å^2), and limited hydrogen-bonding capacity. In contrast, smaller compounds, such as 5-hydroxymethylfurfural, catechol, furaneol, and maltol, demonstrated significantly higher solubility (logS near 0), making them more suitable for oral absorption. Quinic acid showed the highest polarity (TPSA 118.22 Å^2) and the highest H-bonding potential (nHA/nHD 6/5), suggesting excellent interaction capacity but reduced permeability. Squalene displayed extreme lipophilicity (logP 11.16) and a zero TPSA, making it unsuitable as an orally bioavailable drug, despite its strong docking affinity. Overall, smaller hydrophilic molecules, such as maltol, catechol, and 5-HMF, exhibited more favorable physicochemical behavior than the native ligand. Drug-likeness evaluation showed that all compounds, including the native ligand, complied with Lipinski's rule (Table 5).

Table 5. Drug-likeness properties of designed derivatives

Compounds	QED	NP Score	Lipinski rule	Pfizer rule	GSK rule	Golden triangle	Chelator rule
NL-2WGE	0.712	2.225	0	0	0	0	0
5-Hydroxymethylfurfural	0.59	0.618	0	0	0	1	0
Catechol	0.491	0.521	0	0	0	1	1
Furaneol	0.524	1.156	0	0	0	1	0
Hydroquinone	0.491	0.593	0	0	0	1	0
Loliolide	0.596	2.982	0	0	0	1	0
Maltol	0.555	0.919	0	0	0	1	1
Methyl_*N*-hydroxybenzenecarboximidate	0.286	-0.118	0	0	0	1	0
Phenol, 3,4,5-trimethyl-	0.58	0.489	0	0	0	1	0
Quinic_acid	0.318	2.249	0	0	0	1	0
Squalene	0.186	0.956	0	1	1	1	0

Quality drug-likeness (QED) values indicated that NL-2WGE (0.712) had the highest score; however, several phytochemicals also showed good scores, particularly loliolide (0.596), 5-HMF (0.59), and phenol-3,4,5-trimethyl (0.58). Loliolide and quinic acid exhibited high NP scores (2.98 and 2.24, respectively), reflecting strong natural-product-like complexity, which is advantageous in lead discovery. Except for squalene, all compounds passed the Pfizer and GSK toxicity filters, suggesting a lower likelihood of toxicity-related attrition. The Golden Triangle rule was satisfied by all compounds, indicating that their mass–lipophilicity balance is favorable for oral drugs. Overall, loliolide, maltol, and 5-HMF demonstrated better drug-likeness than the native ligand.

NL-2WGE showed moderate permeability (Caco-2 and MDCK values near –4.7) and low Human Intestinal Absorption (HIA) (0.0159). Many phytochemicals exhibited significantly improved absorption characteristics (Table 6). Catechol, loliolide, and 5-HMF had higher HIA values, indicating better intestinal uptake. Loliolide showed the strongest overall oral absorption profile, with a high HIA (0.37) and excellent predicted oral bioavailability (F20–F50 >0.87). Most compounds did not behave strongly as P-gp inhibitors or substrates, lowering the efflux-related failure risk; the exceptions were squalene and quinic acid, which showed P-gp substrate tendencies. Furaneol and hydroquinone showed relatively lower absorption values than other compounds. Overall, loliolide, catechol, and 5-

HMF outperformed the native ligand in terms of the absorption potential.

NL-2WGE exhibited high plasma protein binding (PPB, 95.8%), leaving a very low free fraction (Fu, 3.46%), which may limit its bioavailability. Many phytochemicals displayed lower PPB values, especially quinic acid (23.9%) and hydroquinone (24.1%), indicating a higher freely available drug concentration in plasma compared to the native ligand (Table 7). BBB penetration remained low for most compounds, except phenol-3,4,5-trimethyl and methyl-hydroxybenzenecarboximidate, which showed high BBB values. CYP450 analysis revealed that quinic acid had minimal interaction with metabolic enzymes, suggesting excellent metabolic safety.

Table 6. Absorption parameter of selected compounds

Compounds	Caco-2 Permeability	MDCK Permeability	Pgp-inhibitor	Pgp-substrate	HIA	F20%	F30%	F50%
NL-2WGE	-4.7103	-4.7024	0.54575	0.08048	0.01595	0.60714	0.88046	0.967
5-Hydroxymethylfurfural	-4.8706	-4.6244	0.13018	0.02663	0.1277	0.74583	0.87142	0.57289
Catechol	-4.8288	-4.7185	0.01733	0.0747	0.1398	0.82774	0.87779	0.93303
Furaneol	-4.5551	-4.6247	0.22243	0.11059	0.12863	0.23836	0.51212	0.79197
Hydroquinone	-5.0778	-4.7398	0.01824	0.01453	0.00169	0.36415	0.28635	0.70388
Loliolide	-4.9256	-4.7598	0.36827	0.28399	0.37652	0.95783	0.87566	0.97741
Maltol	-4.7862	-4.7493	0.37483	0.20563	0.16839	0.30644	0.50115	0.52045

Methyl_*N*-hydroxybenzenecarboximidate	-4.3965		-4.6888		0.10324		0.02795		0.01323		0.14319		0.28003		0.77444	
Phenol, 3,4,5-trimethyl-	-4.5889		-4.7245		0.02461		0.05997		0.00044		0.08294		0.12006		0.81038	
Quinic_acid	-5.9983		-4.8368		2.93E-07		0.57756		0.04651		0.23925		0.29422		0.92454	
Squalene	-4.5925		-4.7641		1		1.33E-05		0.0114		0.00024		0.0008		0.63866	

Table 7. Distribution and metabolism parameter of selected molecules

Compounds	Distribution				Metabolism											
					CYP1A2		CYP2C19		CYP2C9		CYP2D6		CYP3A4	
	PPB%	VD	BBB	Fu	Inhibitor	Substrate	Inhibitor	Substrate	Inhibitor	Substrate	Inhibitor	Substrate	Inhibitor	Substrate
NL-2WGE	95.8352	0.36382	0.03441	3.46106	0.1495	0.13525	0.53938	0.02073	0.33712	0.89003	0.0007	0.05525	0.04424	0.34582
5-Hydroxymethylfurfural	20.4917	0.08144	0.38474	80.7417	0.97559	0.24634	0.50181	0.0306	0.92353	0.92885	0.13954	0.89216	0.02892	0.79649
Catechol	57.4016	-0.281	0.55548	35.0016	0.51002	0.1241	0.1247	0.04996	0.05843	0.33844	0.00753	0.93441	0.13393	0.01109
Furaneol	40.4569	-0.1722	0.36302	55.3233	0.78022	0.93241	0.92495	0.59909	0.21457	0.12538	0.00097	0.00028	0.12655	0.2667
Hydroquinone	24.1663	-0.0282	0.02591	68.3249	0.78921	0.04214	0.03842	0.03837	0.05912	0.36789	0.11763	0.99019	0.0853	0.06515

Loliolide	73.277	-0.1171	0.19008	25.103	0.0001	0.0151	0.02206	0.79358	0.44198	0.10894	0.0679	2.16E-05	0.87229	0.73384
Maltol	51.389	-0.2047	0.42091	43.8375	0.71514	0.56401	0.54144	0.64002	0.15408	0.82678	0.00122	0.82915	0.0059	0.63517
Methyl_*N*-hydroxybenzenecarboximidate	91.9544	-0.7174	0.82842	7.1647	0.63506	0.00108	0.61201	8.16E-07	0.96637	0.0162	0.0144	0.13139	0.00061	0.90191
Phenol, 3,4,5-trimethyl-	85.555	0.1622	0.86896	12.8388	0.99779	0.9997	0.99927	0.80912	0.55965	0.98898	0.01497	0.99954	0.62747	0.9998
Quinic_acid	23.9877	-0.459	0.00421	77.6888	7.71E-08	4.54E-09	5.39E-07	9.75E-07	1.22E-06	0.01154	1.98E-05	6.86E-09	5.59E-07	6.14E-05
Squalene	96.3837	-0.0728	0.00122	3.13571	0.00231	0.00012	0.95846	0.99947	0.05597	0.88623	0.00156	0.99962	0.93523	6.10E-05

Conversely, squalene showed broad CYP inhibition/substrate liability, indicating its metabolic instability. Overall, quinic acid and loliolide demonstrated safer and more balanced distribution–metabolism profiles than the native ligand. Many compounds showed longer predicted half-lives than NL-2WGE (T½ = 0.89 h). Quinic acid (T½ = 3.50 h), catechol (2.16 h), and maltol (2.08 h) demonstrated longer systemic retention, which may support improved therapeutic coverage. Toxicity parameters showed that several phytochemicals, including quinic acid, squalene, and phenol-3,4,5-trimethyl, exhibited significantly lower hepatotoxicity and carcinogenicity than their native ligands. Quinic acid displayed the lowest toxicity profile across most endpoints, including Drug-Induced Liver Injury (DILI), Ames, FDA Maximum (recommended) Daily Dose database (FDAMDD), and carcinogenicity, making it the safest compound in the dataset. Catechol and hydroquinone showed slightly elevated toxicity in some parameters but remained within acceptable ranges. Overall, quinic acid and squalene demonstrated the safest toxicity profiles, and quinic acid was superior to NL-2WGE. The excretion and toxicity parameters of the selected compounds and NL-2WGE are presented in Table 8.

Table 8. Excretion and toxicity parameters of selected compounds

Compounds	Excretion		Toxicity								
	CL-plasma	T1/2	H-HT	DILI	Ames toxicity	Rat oral acute toxicity	FDAMDD	Skin sensitization	Carcinogenicity	Eye corrosion	Eye irritation	Respiratory toxicity
NL-2WGE	5.79285	0.891	0.56791	0.82729	0.42363	0.44527	0.2406	0.9859	0.51949	0.60663	0.97876	0.86425
5-Hydroxymethylfurfural	8.75156	1.0885	0.33289	0.84846	0.80749	0.42667	0.29077	0.84338	0.93806	0.89908	0.9923	0.68733
Catechol	16.166	2.16106	0.34348	0.18484	0.58874	0.54241	0.5721	0.99541	0.76244	0.99225	0.99867	0.72599
Furaneol	2.94798	2.58127	0.61582	0.80503	0.62925	0.40379	0.1848	0.93498	0.68984	0.88842	0.98987	0.45236
Hydroquinone	17.0429	1.76502	0.39216	0.1825	0.51845	0.55322	0.48959	0.98726	0.75001	0.99107	0.99827	0.66577
Loliolide	7.39474	1.56792	0.64758	0.34381	0.803	0.65275	0.68963	0.98456	0.84359	0.37215	0.94945	0.53882
Maltol	7.63759	2.08387	0.40455	0.44287	0.64318	0.55711	0.57652	0.29233	0.7303	0.75295	0.99099	0.72529
Methyl_*N*-hydroxybenzenecarboximidate	3.38884	1.73508	0.89323	0.55003	0.66875	0.19004	0.18936	0.90519	0.75623	0.93713	0.99733	0.82768
Phenol, 3,4,5-trimethyl-	10.3041	1.29428	0.58316	0.27832	0.58536	0.36473	0.38307	0.82922	0.77059	0.98739	0.99818	0.78175

Quinic_acid	1.36086	3.50935	0.50387	0.10238	0.30908	0.09079	0.16233	0.42795	0.34803	0.03398	0.86726	0.19328
Squalene	10.2798	0.64095	0.79498	0.01272	0.01073	0.04909	0.11246	0.9988	0.02375	0.1184	0.94807	0.98617

Table 9. Environmental toxicity profile of designed molecules

Compounds	BCF	IGC_{50}	$LC_{50}FM$	$LC_{50}DM$
NL-2WGE	1.03494	3.56697	4.65324	5.33709
5-Hydroxymethylfurfural	0.37813	2.94985	3.45265	4.01379
Catechol	1.33089	3.72309	4.32039	4.58798
Furaneol	0.41414	2.96988	3.3301	4.09645
Hydroquinone	1.36949	3.50078	3.94996	4.38604
Loliolide	0.29825	2.89736	3.48992	4.23114
Maltol	0.71796	3.14663	3.18243	3.93414
Methyl_*N*-hydroxybenzenecarboximidate	0.39844	2.86503	3.2532	4.06075
Phenol, 3,4,5-trimethyl-	1.41651	3.9353	4.29438	4.72067
Quinic_acid	0.22518	2.14051	2.87825	3.36977
Squalene	1.39902	5.5531	7.94353	7.37865

Table 10. ADMET radar summary highlighting key pharmacokinetic and drug-likeness parameters of the most potent phytochemicals in comparison with the native ligand

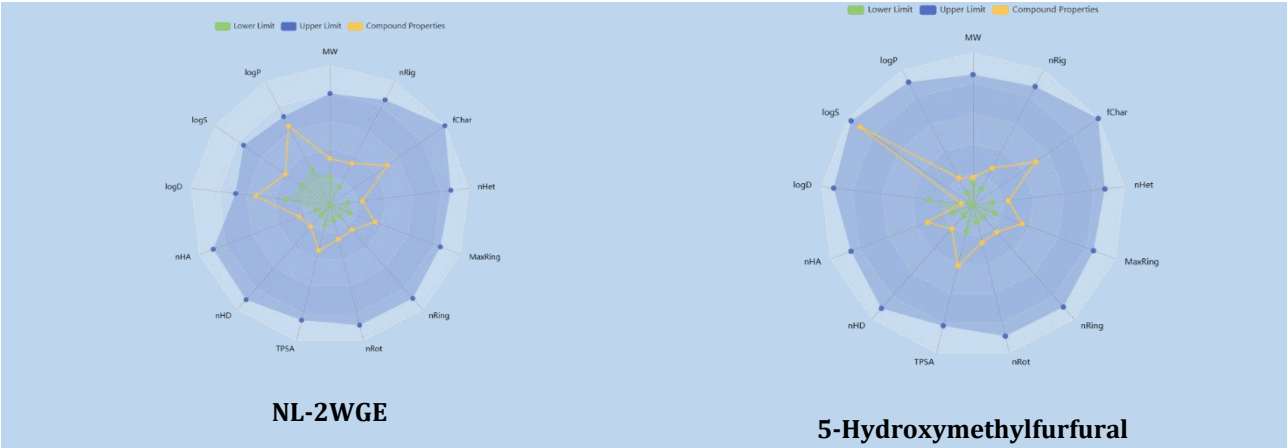

NL-2WGE **5-Hydroxymethylfurfural**

Catechol **Furaneol**

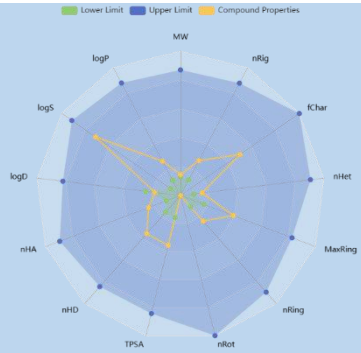

Hydroquinone

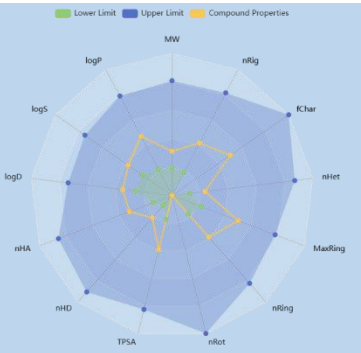

Loliolide

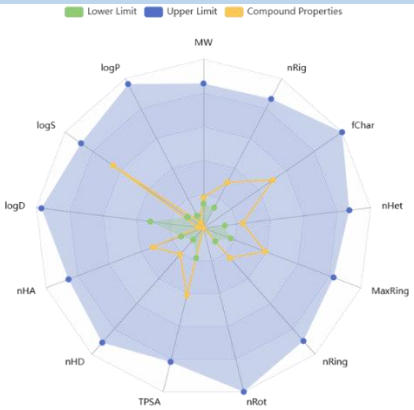

Maltol

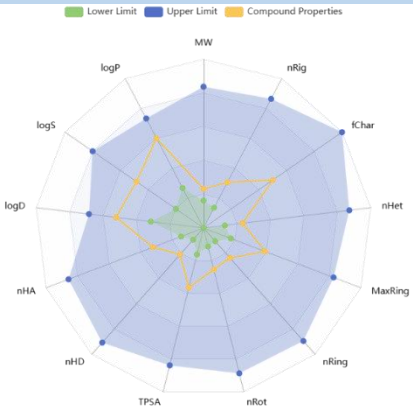

Methyl_*N*-hydroxybenzenecarboximidate

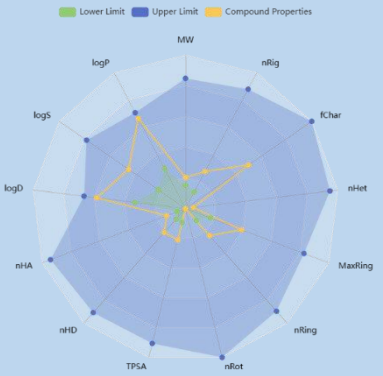

Phenol, 3,4,5-trimethyl-

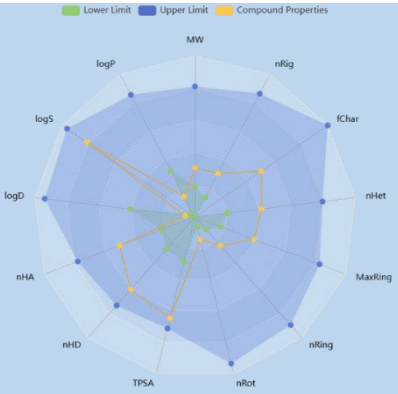

Quinic_acid

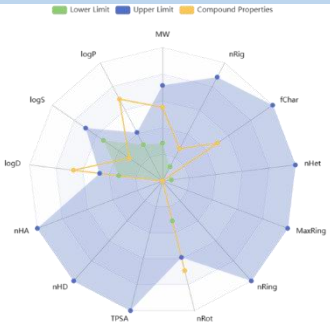

Squalene

Environmental toxicity analysis showed that most compounds displayed moderate to low bioaccumulation factors (BCF) (Table 9). Quinic acid (0.22) and loliolide (0.29) showed the lowest BCF values, suggesting minimal environmental persistence. Despite its high hydrophobicity, squalene showed the least aquatic toxicity based on LC_{50} and IGC_{50} indices; although its high BCF indicates environmental accumulation risk. Catechol and phenol-3,4,5-trimethyl showed higher BCF values, but remained within acceptable environmental safety limits. ADMET radar of all potent compounds and native ligand are depicted in Table 10. Overall, quinic acid and loliolide exhibited the most favorable environmental toxicity profiles.

Conclusion

The present study demonstrates that the hydroalcoholic extract of *Cissus verticillata* is pharmaceutically acceptable, chemically rich, and computationally promising against Mycobacterium tuberculosis. Organoleptic and physicochemical evaluations confirmed a stable, neutral extract with good yield, appropriate moisture content, and absence of foreign matter, heavy metals, pesticides, and pathogenic bacteria, indicating suitability for further therapeutic development. Preliminary phytochemical screening revealed abundant alkaloids, flavonoids, and phenolic compounds, along with moderate levels of saponins and tannins, indicating strong antioxidant, antimicrobial, and anti-inflammatory potential. GC–MS profiling further confirmed a diverse array of bioactive compounds, dominated by cyclic dipeptides (L-prolyl-L-valine, 3,6-diisopropylpiperazin-2,5-dione) and phenolic constituents (hydrocinnamic acid, tyrosol, and benzeneacetic acid), which together underpin the multifaceted bioactivity of the extract. Molecular docking identified several compounds, particularly loliolide, quinic acid, methyl-*N*-hydroxybenzenecarboximidate, and squalene, with binding affinities comparable to or exceeding those of the native ligand of the 2WGE target, engaging key hydrophobic and hydrogen-bonding hotspots. The ADMET analysis highlighted loliolide, maltol, 5-hydroxymethylfurfural, and quinic acid as drug-like, orally favorable, and relatively safe, with acceptable toxicity and environmental profiles. Overall, *Cissus verticillata* has emerged as a valuable source of anti-tubercular lead candidates, warranting targeted isolation, *in vitro* validation, and further optimization.

Disclosure Statement

No potential conflict of interest was reported by the authors.

ORCID

Sanjay Kumar Nayak:
https://orcid.org/0009-0002-7312-9043
Neelam Sharma:
https://orcid.org/0009-0004-3463-8392
Ganesh Meena B.:
https://orcid.org/0009-0006-8817-935X
Yaso Deepika Mamidisetti:
https://orcid.org/0000-0002-4141-2285
Rashmi Ranjan Sarangi:
https://orcid.org/0000-0002-8980-4675
Rajendra Kumar Jadi:
https://orcid.org/0000-0002-9039-8061
Murugesan Sudha:
https://orcid.org/0009-0003-2987-2531
Divya Amaravadi:
https://orcid.org/0000-0001-9945-4501
Jainendra Kumar Battineni:
https://orcid.org/0000-0003-1229-4686

References

[1] Maison, D.P. Tuberculosis pathophysiology and anti-VEGF intervention. *Journal of Clinical Tuberculosis and Other Mycobacterial Diseases*, **2022**, 27, 100300.

[2] Daniel, T.M., Bates, J.H., Downes, K.A. History of tuberculosis. *Tuberculosis: Pathogenesis, Protection, and Control*, **1994**, 13-24.
[3] Chowdhury, K., Ahmad, R., Sinha, S., Dutta, S., Haque, M. Multidrug-resistant tb (MDR-TB) and extensively drug-resistant tb (XDR-TB) among children: Where we stand now. *Cureus*, **2023**, 15(2).
[4] Saderi, L., Cabibbe, A., Puci, M., Di Lorenzo, B., Centis, R., Pontali, E., Van den Boom, M., Chakaya, J., Denholm, J., Ferrara, G. A systematic review of the costs of diagnosis for multidrug-resistant/extensively drug-resistant tb in different settings. *The International Journal of Tuberculosis and Lung Disease*, **2023**, 27(5), 348-356.
[5] Migliori, G.B., Dheda, K., Centis, R., Mwaba, P., Bates, M., O'Grady, J., Hoelscher, M., Zumla, A. Review of multidrug-resistant and extensively drug-resistant tb: Global perspectives with a focus on sub-saharan africa. *Tropical Medicine & International Health*, **2010**, 15(9), 1052-1066.
[6] Rojas-Sandoval, J. Cissus verticillata (possum grape vine). CABI Compendium: Wallingford, UK. **2022**.
[7] Drobnik, J., de Oliveira, A.B. Cissus verticillata (l.) nicolson and ce jarvis (vitaceae): Its identification and usage in the sources from 16th to 19th century. *Journal of Ethnopharmacology*, **2015**, 171, 317-329.
[8] Beltrán-Melgarejo, A., Vargas-Mendoza, M.d.l.C., Pérez-Vázquez, A., García-Albarado, J.C. Thermal comfort of green roofs with cissus verticillate (vitaceae) in tropical rural dwellings. *Revista Mexicana de Ciencias Agrícolas*, **2014**, 5(SPE9), 1551-1560.
[9] Souza Neto, A.A., Diniz Melquiades de Medeiros, L.A., Lia Fook, M.V., de Siqueira, R.R., Barbosa, R.C., Antas de Moraes, W.G., Rosendo, R.A. Development and characterization of membranes of chitosan/cissus verticillata (L.) nicolson & CE jarvis. *Materia-Rio De Janeiro*, **2019**, 24(3).
[10] Paiva, E.A.S., Buono, R.A., Lombardi, J.A. Food bodies in cissus verticillata (vitaceae): Ontogenesis, structure and functional aspects. *Annals of Botany*, **2009**, 103(3), 517-524.
[11] Silva, L.d., Oniki, G.H., Agripino, D.G., Moreno, P.R., Young, M.C.M., Mayworm, M.A.S., Ladeira, A.M. Biciclogermacreno, resveratrol e atividade antifúngica em extratos de folhas de cissus verticillata (l.) nicolson & jarvis (vitaceae). *Revista Brasileira de Farmacognosia*, **2007**, 17, 361-367.
[12] Valdez, C.A. Gas chromatography-mass spectrometry analysis of synthetic opioids belonging to the fentanyl class: A review. *Critical Reviews in Analytical Chemistry*, **2022**, 52(8), 1938-1968.
[13] Gould, O., Nguyen, N., Honeychurch, K.C. New applications of gas chromatography and gas chromatography-mass spectrometry for novel sample matrices in the forensic sciences: A literature review. *Chemosensors*, **2023**, 11(10), 527.
[14] Lima, C.C., Silva, D.S.N., de Sá, É.R.A. Computational analysis of sulfonamide-based compounds by molecular docking and adme/t in the inhibition of acetylcholinesterase (ache) in alzhaimer's disease. *Open Access Library Journal*, **2022**, 9(3), 1-13.
[15] Laskar, Y.B., Mazumder, P.B., Talukdar, A.D. Hibiscus sabdariffa anthocyanins are potential modulators of estrogen receptor alpha activity with favourable toxicology: A computational analysis using molecular docking, adme/tox prediction, 2d/3d qsar and molecular dynamics simulation. *Journal of Biomolecular Structure and Dynamics*, **2023**, 41(2), 611-633.
[16] Khan, S., Kale, M., Siddiqui, F., Nema, N. Novel pyrimidine-benzimidazole hybrids with antibacterial and antifungal properties and potential inhibition of sars-cov-2 main protease and spike glycoprotein. *Digital Chinese Medicine*, **2021**, 4(2), 102-119.
[17] Mohammed, S., Abdulmalik, I., Abdulkadir, F. Investigation of chemical fraction of nickel in maize and soil using the cold extraction technique. *Advance Journal of Food Science and Technology*, **2013**, 5(2), 137-143.
[18] Nahor, E.M., Rumagit, B.I., Tou, H.Y. Perbandingan rendemen ekstrak etanol daun andong (cordyline futicosa l.) menggunakan metode ekstraksi maserasi dan sokhletasi. *Prosiding Seminar Nasional Tahun 2020 ISBN: 978-623-93457-1-6*, **2020**, 40-44.
[19] Sapiun, Z., Pangalo, P., Imran, A.K., Wicita, P.S., Daud, R.P.A. Determination of total flavonoid levels of ethanol extract sesewanua leaf (clerodendrum fragrans wild) with maceration method using uv-vis spectrofotometry. *Pharmacognosy Journal*, **2020**, 12(2).
[20] Sahumena, M.H., Zubaydah, W.S., Jannah, S.R.N., Mardikasari, S.A., Aswan, M., Maria, S.F., Adjeng, A.N.T., Nisa, M. Formulation and physicochemical evaluation of theophylline nanoparticles transdermal patch. *Egyptian Journal of Chemistry*, **2022**, 65(132), 51-57.
[21] Kripa, K., Sangeetha, R., Chamundeeswari, D. Pharmacognostical and physicochemical evaluation of the plant leucas aspera. *Asian Journal of Pharmaceutical and Clinical Research*, **2016**, 9, 263-268.
[22] Ismail, A.M., Mohamed, E.A., Marghany, M.R., Abdel-Motaal, F.F., Abdel-Farid, I.B., El-Sayed, M.A. Preliminary phytochemical screening, plant growth inhibition and antimicrobial activity studies of faidherbia albida legume extracts. *Journal of the Saudi Society of Agricultural Sciences*, **2016**, 15(2), 112-117.

[23] Yadav, M., Chatterji, S., Gupta, S.K., Watal, G. Preliminary phytochemical screening of six medicinal plants used in traditional medicine. *International Journal of Pharmacy and Pharmaceutical Sciences*, **2014**, 6(5), 539-542.
[24] Geletu, U.S., Usmael, M.A., Ibrahim, A.M. Isolation, identification, and susceptibility profile of e. Coli, salmonella, and s. Aureus in dairy farm and their public health implication in central ethiopia. *Veterinary Medicine International*, **2022**, 2022(1), 1887977.
[25] Shekar, A., Babu, L., Ramlal, S., Sripathy, M.H., Batra, H. Selective and concurrent detection of viable salmonella spp., E. Coli, staphylococcus aureus, e. Coli o157: H7, and shigella spp., in low moisture food products by pma-mpcr assay with internal amplification control. *LWT*, **2017**, 86, 586-593.
[26] Pai, A., Shenoy, C. Physicochemical, phytochemical, and gc–ms analysis of leaf and fruit of pouteria campechiana (kunth) baehni. *Journal of Applied Biology and Biotechnology*, **2020**, 8(04), 90-97.
[27] Mlozi, S.H., Mmongoyo, J.A., Chacha, M. Gc-ms analysis of bioactive phytochemicals from methanolic leaf and root extracts of tephrosia vogelii. *Scientific African*, **2022**, 16, e01255.
[28] Ezhilan, B.P., Neelamegam, R. Gc-ms analysis of phytocomponents in the ethanol extract of polygonum chinense l. *Pharmacognosy Research*, **2012**, 4(1), 11.
[29] Jadhav, S., Dighe, P. Synthesis, in vitro evaluation, and molecular docking studies of novel pyrazoline derivatives as promising bioactive molecules. *Journal of Pharmaceutical Sciences and Computational Chemistry,* **2025**, 1(3), 190-209.
[30] Siddiqui, F., Makhloufi, R., Salah, M.E.-S., Mohamed, E., Hojjati, M. Computational exploration of quinine and mefloquine as potential anti-malarial agents. *Journal of Pharmaceutical Sciences and Computational Chemistry*, **2025**, 1(2), 106-115.
[31] Ahmed, S., Tabassum, P., Falak, S., Ahmad, A., Shaikh, M. Molecular docking and network pharmacology: Investigating vitis vinifera phytoconstituents as multi-target therapeutic agents against breast cancer. *Journal of Pharmaceutical Sciences and Computational Chemistry,* **2025**, 1(2), 116-134.
[32] Tamboli, A., Tayade, S. In-depth investigation of berberine and tropane through computational screening as possible dpp-iv inhibitors for the treatment of T2DM. *Journal of Pharmaceutical Sciences and Computational Chemistry*, **2025**, 1(1), 1-11.
[33] Reddy, K.K., Arjun, U.N.V., Alhmoud, J.F., Reddy, S.M., Dhillishree, D., Tambe, V.B., Shinde, G.S., Shanmugarajan, T.S., Dharmamoorthy, G., Gobalakriahnan, P. In depth in silico exploration of some natural indole alkaloids as potential plasmepsin ii inhibitors: Admet calculations, molecular docking analysis, molecular dynamics simulation, and DFT studies. *Chemical Methodologies*, **2025**, 9, 277-300.
[34] Chinnakadoori, S.R., Reddy, S.M., Bodapati, A., Kallam, S.D.M., Dharmamoorthy, G., Gupta, J.K., Asha, P., Arjun, U.V.N.V., Alja'afreh, A.A., Abu, W. Biological exploration of substituted-phenyl-1h-pyrazol-4-yl) methylene) aniline derivatives as potential dpp-iv inhibitors: Admet screening, molecular docking, and dynamics simulations. *Chemical Methodologies*, **2025**. **2025**, 9(1), 52–80.

HOW TO CITE THIS ARTICLE

S.K. Nayak, N. Sharma, G. Meena B., Y.D. Mamidisetti, R.R. Sarangi, R.K. Jadi, M. Sudha, D. Amaravadi, J.K. Battineni. Phytochemical Profiling and Computational Assessment of *Cissus Verticillata* Bioactives Using GC–MS Against *Mycobacterium Tuberculosis*. *Adv. J. Chem. A*, 2026, 9(6), 1087-1111.

DOI: 10.48309/ajca.2026.561857.1978
URL: https://www.ajchem-a.com/article_238862.html